Struct Multidisc Optim (2016) 53:801–811
DOI 10.1007/s00158-015-1365-2

RESEARCH PAPER

Optimal layout of multiple bi-modulus materials

Kun Cai[1,2] **· Jing Cao**[1] **· Jiao Shi**[1] **· Lingnan Liu**[1] **· Qing H. Qin**[2]

Received: 4 May 2015 / Revised: 19 October 2015 / Accepted: 21 October 2015 / Published online: 20 November 2015

Abstract A modified solid isotropic material with penalization (SIMP) method is proposed for solving layout optimization problems of multiple bi-modulus materials in a continuum. In the present algorithm, each bi-modulus material is replaced by two distinct isotropic materials to avoid structural reanalysis for each update of the design domains. To reduce the error in local stiffness due to the material replacement, the modification factor of each finite element is calculated according to the local stress state and the moduli used in the previous structural analysis. Three numerical examples are considered to demonstrate the validity and applicability of the present approach. Numerical results show that the final layout of materials is determined by factors that include the moduli difference of each bi-modulus material and the difference among material moduli.

Keywords Topology optimization · Multi-material structures · Bi-modulus material · SIMP · Material replacement · Isotropic material

1 Introduction

Topology optimization has become popular in the field of design and manufacturing of complex structures attributed to the associated well-developed theory of optimization (Bendsoe and Sigmund 2003; Cai et al. 2014a, b, c; Eschenauer and Olhoff 2001; Guo et al. 2014a; Rodriguez-Velazquez and Seireg 1985; Rozvany et al. 1995; Sigmund 1994; Wang et al. 2003; Xie and Steven 1993) and the rapid development of high-performance computing (HPC). Topological optimization is an especially powerful tool in the concept design phase. It has been used in the design of micro-electro-mechanical systems (MEMS) (Luo et al. 2009; Maute and Frangopol 2003), acoustic devices (Dühring et al. 2008), fluidics devices (Andreasen et al. 2009), functional materials (Diaz and Sigmund 2010), structures associated with heat conduction problems (Zhuang et al. 2007, 2010), optimal bone structures (Shi et al. 2014), and lightweight structures (Cai and Qin 2012). It is worth mentioning that several typical methods for continuum topology optimization play an important role in the application of topology optimization to practical engineering design. For instance, the ground structure method (Dorn 1964) offered a feasible way to find an optimal load path in a continuum that is replaced by a truss structure. As a milestone work in continuum topology optimization, the homogenization-based design method (Bendsoe and Sigmund 2003) for topology optimization was proposed at the end of the 1980s. It is now a powerful approach for the design of composite materials. In early 1990s, the method of solid isotropic material with penalization (SIMP) (Zhou and Rozvany 1991) and the method of evolutionary structural optimization (ESO) (Alfieri et al. 2007; Guan et al. 1999; Xie and Steven 1993, 1997) were developed. These methods featured widely across applications in engineering design and analysis due to their simplicity and high efficiency. The level set method (LSM), adopted in topology optimization after 2000 (Allaire et al. 2004; Norato et al. 2015; Osher and Santosa 2001; Wang et al. 2003, 2015) has attracted much attention, especially in the optimization of multiple-material layouts.

✉ Qing H. Qin
qinghua.qin@anu.edu.au

[1] College of Water Resources and Architectural Engineering, Northwest A&F University, Yangling 712100, China

[2] Research School of Engineering, Australian National University, Acton, ACT 2601, Australia

In most practical engineering a structure/device/composite consists of more than one material. Thus, development of the theory of topology optimization for the design of multiple-material layouts is of significance and, over the last two decades, many techniques have been developed for solving this problem, such as solution methods based on the SIMP method (Gibiansky and Sigmund 2000; Sigmund and Torquato 1999), LSM based work (Allaire et al. 2014; Mei and Wang 2004; Wang and Wang 2004), ESO method based approach (Han and Lee 2005; Huang and Xie 2010), the discrete material optimization (DMO) approach (Blasques and Stolpe 2012; Hvejsel and Lund 2011; Stegmann and Lund 2005), and phase field method (Wang and Zhou 2004; Zhou and Wang 2007). The method presented by Ramani, termed the ‘pseudo-sensitivities’ approach, can also be used to find the optimal layouts of materials in a large structure (Ramani 2010). Different from the approaches mentioned above, Guo et al. (2014b) suggested a structural optimization method based on moving morphable components. Using the method, one can provide not only the layouts of components, but the detailed sizes and shapes of components in the final design. When the components are specified with different materials, the final design is a typical layout of multiple materials.

The works cited above focus mainly on finding the optimal distribution of multiple isotropic material layouts. However, if the behavior of materials is bi-modulus, i.e., the tensile modulus is different from the compressive modulus along the same direction (Du and Guo 2014), the multiple bi-modulus materials layout optimization problem becomes complex when using structural reanalysis for finding the accurate deformation field for each update of design variables. Actually, bi-modulus is very common in engineering, and is found in rubber, concrete, cast iron, graphite (Seldin 1966), foam materials (Xiao and Qin 2013; Zenkert and Burman 2009), masonry (Kanno 2011; Stimpson and Chen 1993), bone (Qin and Ye 2004; Qin et al. 2005; Zhu et al. 2006), alloys (Liu et al. 1998), membranes (Mosler/membranes (Mosler and Cirak 2009; Roddeman et al. 1987), and so on. Due to the stress-dependency of the constitutive properties of a bi-modulus material, the deformation analysis theory for bi-modulus structures has attracted considerable attention since 1960s (Ambartsumyan 1965; Du and Guo 2014; Jones 1977; Kanno 2011). During that period, topology optimization of bi-modulus material structures was also performed. For example, Achtziger (1996) adopted a ground structure approach to find the optimal topology of a truss with different properties of tension and compression. Comparisons of the numerical results showed that the final structure under tension was obviously different from the structure under compression. Chang et al. (2007) proposed an approximation approach for optimization of structures containing tension-only or compression-only material. In their approach, the original piece-wise linear stress-strain curve of bi-modulus material was approximated with a derivable nonlinear curve. Similarly, Liu and Qiao (2011) proposed a modified Heaviside function to approximate the piece-wise linear curve in optimization of bi-modulus structures. Cai et al. (2014d) proposed a bionics method as well as a reference interval method based on bone remodeling methodology for topology optimization with tension/compression -only materials. In strength design, Bruggi and Duysinx (2013) presented a stress-based approach to address the truss-like elastic structures with unilateral material. In the work, Drucker–Prager criterion was adopted to provide a smooth approximation. Bruggi (2014) proposed an alternative numerical approach of energy–based method for analysing no–tension masonry–like solids. Yang et al. (2015) used a hybrid truss-continuum model to capture tensile forces in steel and the compressive forces in concrete. Guo et al. (2014a) discussed the layout optimization of multiple materials with stress-constraint. Recently, Baratta et al. (2015) proposed an analytical formulation of generalized incremental theorems of no-tension bodies. Cai (2011) suggested a material replacement scheme in the modified SIMP method for topological design with tension-only or compression-only materials. Querin et al. (2010) used orthotropic materials to replace original bi-modulus material according to the local stress state in topology optimization of truss-like structures. In the work reviewed above, the constitutive of bi-modulus is usually approximated in some way in structural analysis. Making use of the variational principles, Du and Guo (2014) proposed a more efficient and accurate deformation model of a bi-modulus structure for stress analysis. Recently, Cai et al. (2013) suggested a simpler scheme for finding the optimal topology of a bi-modulus structure. In their work, the original bi-modulus material was replaced by two isotropic materials. The moduli of the two isotropic materials were identical to those of the bi-modulus material. In deformation analysis, the appropriate modulus was chosen for an element according to the local stress state. To reduce the variation of local stiffness due to material replacement, a modification factor of local stiffness was calculated. The validity of the method was well demonstrated in the numerical results. It should be mentioned that only one bi-modulus material was considered in structural optimization in those studies.

In this paper, we present an approach for dealing with layout optimization associated with multiple bi-modulus materials. In the optimization model, the objective is to minimize the mean structural compliance of structures with multiple bi-modulus materials. This article is organized as follows. In Section 2, a bi-modulus material is defined. In Section 3, the present algorithm method is detailed. In Section 4, three representative numerical examples are presented to demonstrate the validity and applicability of this method. Finally, some conclusions are presented.

2 Model for bi-modulus material

From the stress-strain curve of a bi-modulus material shown in Fig. 1, where the tensile modulus ($E_T = \tan\alpha$, $\alpha \in [0, \ 90^\circ)$) and compressive modulus ($E_C = \tan\beta$, $\beta \in [0, \ 90^\circ)$) are displayed in blue and red respectively, we find that (a) $\alpha=\beta$ for isotropic materials; (b) $\alpha \neq \beta$ for bi-modulus materials; (c) $\beta=0$ for tensile-only materials; and (d) $\alpha=0$ for compressive-only materials. σ_T and σ_C are the allowable stresses under tension and under compression of the material, respectively.

When the material is under three-dimensional stress state, the constitutive relation between the stress and strain tensors is classified, separately. For instance, (a) if all the principal stresses are positive, the isotropic elastic tensor with tensile modulus and tensile Poisson's ratio should adopted. The two material constants can be obtained by one-dimensional tensile experiment; (b) if all the principal stresses are negative, the isotropic elastic tensor with compressive modulus and compressive Poisson's ratio should be adopted; (c) if the second principal stress is positive and the third one is negative, a transversally isotropic elastic tensor should be used and the material principal direction normal to the isotropic plane is align with that of the third principal stress; (d) if the second principal stress is negative and the first one is positive, the transversally isotropic elastic tensor should be used and the material principal direction is align with that of the first principal stress.

To represent the difference between the tension and compression performance for bi-modulus materials, we define the ratio between the two moduli as

$$R_{TCE} = \frac{E_T}{E_C}. \tag{1}$$

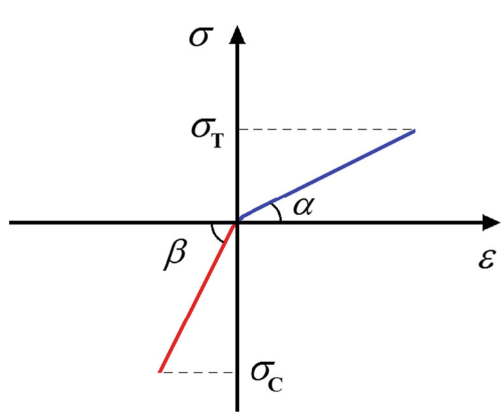

Fig. 1 Stress-strain curve for a bi-modulus material

3 Methodology

3.1 Basic equations for linear elasticity problem

Figure 2 illustrates an initial design domain and its boundary considered in the process of multi-material topology optimization. In our analysis, only linear elasticity is considered and the control equations of the domain are written as

$$\begin{cases} -\nabla\cdot\boldsymbol{\sigma}(\boldsymbol{u}) = \boldsymbol{f} \quad in \ \Omega, \\ \varepsilon(\boldsymbol{u}) = \frac{1}{2}\left[\nabla\boldsymbol{u} + (\nabla\boldsymbol{u})^T\right], \\ \boldsymbol{\sigma}(\boldsymbol{u}) = \boldsymbol{D} : \varepsilon(\boldsymbol{u}) \end{cases} \tag{2}$$

with the boundary conditions defined as

$$\begin{cases} \boldsymbol{u} = \boldsymbol{u}_0 & on \ \Gamma_1, \\ \boldsymbol{\sigma}(\boldsymbol{u})\cdot\boldsymbol{n} = \boldsymbol{T} & on \ \Gamma_2 \end{cases} \tag{3}$$

where Γ_1 and Γ_2 are the Dirichlet and Neumann boundaries, respectively, and $\Gamma_1 \cup \Gamma_2 = \partial\Omega$, $\Gamma_1 \cap \Gamma_2 = \varnothing$. $\Omega \subseteq R^2$ or R^3 is the design domain, $\boldsymbol{\varepsilon}$ denotes the strain tensor, $\boldsymbol{\sigma}$ is the stress tensor, $\boldsymbol{f}$ is the body force vector on a point, $\boldsymbol{u}$ is the displacement vector, $\boldsymbol{u}_0$ denotes the prescribed displacement on the boundary Γ_1, $\boldsymbol{T}$ is the prescribed boundary force per area on Γ_2, and $\boldsymbol{D}$ is the elastic constant tensor.

3.2 Optimization model

In terms of multiple-material layout optimization, the model can be mathematically expressed as

$$\begin{cases} \textbf{Find} & \{\boldsymbol{\rho}_e = [\rho_1, \ \rho_2, \ \ldots, \ \rho_m]_e | e \in \Omega\} \\ \textbf{min} & c = \boldsymbol{F}^T\cdot\boldsymbol{U}, \\ \textbf{s.t.} & \sum_e \psi_{i, \ e}\cdot v_e - \overline{V}_i = 0, \ (i = 1, \ 2, \cdots, \ m), \\ & \boldsymbol{K}\cdot\boldsymbol{U} = \boldsymbol{F}, \\ & 0 \leq \rho_i \leq 1, \ (i = 1, \ 2, \cdots, \ m) \\ & \psi_{i+1, \ e} = \frac{1-\rho_i}{\rho_i(1-\rho_{i-1})}\psi_{i, \ e} \end{cases} \tag{4}$$

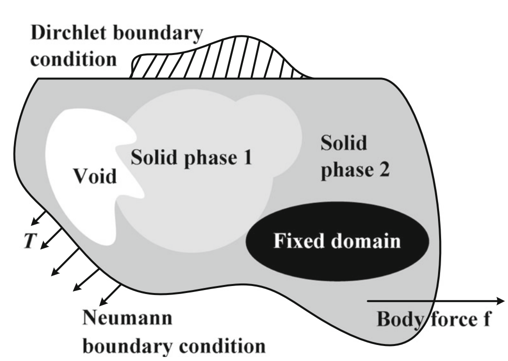

Fig. 2 Schematic of boundary conditions of a continuum with bi-materials

where $\boldsymbol{\rho}_e$ is the design vector of the eth finite element in the design domain. The model contains m elements and is equivalent to the objective that is to minimize the mean compliance of the structure with volume constraints. In (4), v_e is the volume of the eth finite element, $\rho_{i-1,e}$ represents the volume ratio of the first (i-1) materials in the first i materials of the eth finite element. For the case of i=1, ρ_0 is zero. $\psi_{i,\ e}$ is the volume ratio of the ith material in the eth element. $\boldsymbol{F}$ and $\boldsymbol{U}$ denote the global nodal force and global displacement vector respectively. $\overline{V}_i$ is the critical value of the ith material used in the final structure. $\boldsymbol{K}$ is the stiffness matrix, and $\boldsymbol{K}$ and $\boldsymbol{F}$ can be calculated through the well-documented finite element formulation (Bathe 2006; Qin 2000, 2005).

In (4), the density-like method is introduced to show the equivalent elasticity of the composite with multiple materials. For the simplest case, that is, two-material optimization, the equivalent material modulus of the finite element can be expressed as

$$E^{(2)}(\rho_1) = {\rho_1}^p E_1 + (1-{\rho_1}^p)E_2 \tag{5}$$

where $\rho_1 \in [0,1]$ is the design variable of material 1. E_1 and E_2 are the material moduli of the two materials, and p is a constant. Typically, the parameter p= 3 is used.

For a three-phase material layout optimization, the power-law interpolation can be expressed with two design variables ρ_1, ρ_2, i.e.,

$$\begin{aligned} E^{(3)}(\rho_1,\ \rho_2) &= {\rho_2}^p({\rho_1}^p E_1 + (1-{\rho_1}^p)E_2) + (1-{\rho_2}^p)E_3 \\ &= {\rho_2}^p E^{(2)} + (1-{\rho_2}^p)E_3 \end{aligned} \tag{6}$$

where E_3 is the modulus of the third material. The relative density $\rho_1, \rho_2 \in [0,1]$. If there are m materials in the design domain, the equivalent elastic moduli of the composite can be expressed as

$$E^{(m)}(\rho_1, \rho_2, \ldots, \rho_{m-1}) = \rho_{m-1}^p\left(E^{(m-1)}\right) + \left(1-\rho_{m-1}^p\right)E_m. \tag{7}$$

3.3 Material replacement scheme

In Section 3.2, the optimization model and material interpolation scheme are given for finding the optimal layout of multiple isotropic materials. If the materials are bi-modular rather than isotropic or orthotropic, both model and interpolation scheme need to be modified. To extend the application of the model given in (4) to the case of finding optimal bi-modulus materials layout, a material replacement scheme must be carried out before each update of the design variables. Briefly, after the material replacement operation, the original bi-modulus structure becomes a common structure with isotropic materials at the same loading conditions. Hence two major steps must be carried out during material replacement operation. The first is the moduli selection of bi-modulus materials. The second is modification of the local stiffness of the structure with the "new" isotropic materials to approximate the real local stiffness of the structure with the original bi-modulus materials.

3.3.1 Modulus selection

The purpose of the material replacement is to split the structural reanalysis and merge it into the iteration of updating design variables in the process of optimization. Although each bi-modulus material is replaced by two isotropic materials (tension and compressive moduli), in each structural deformation analysis only one modulus is used. Considering the stress-dependency of a bi-modulus, the modulus selection should be carried out according to the local stress state.

For example, considering that σ_s and ε_s (s=1,2,3) are the principal stresses and strains of a finite element in the design domain, the modulus of the rth bi-modulus should be obtained by comparing the tension strain energy densities (SED) and compression SED, i.e.,

$$E_j^r = \begin{cases} E_{\mathrm{T}}^r, & \text{if } SED_{\mathrm{T}} > SED_{\mathrm{C}}, \\ E_{\mathrm{C}}^r, & \text{if } SED_{\mathrm{T}} < SED_{\mathrm{C}},, \\ \max\left(E_{\mathrm{T}}^r, E_{\mathrm{C}}^r\right), & \text{others} \end{cases} \tag{8}$$

where the tension SED and compression SED are defined as

$$SED_{\mathrm{T}} = \frac{\sum\limits_{G_x=1}^{N_G} w_{G_x} \sum\limits_{G_y=1}^{N_G} w_{G_y} \sum\limits_{G_z=1}^{N_G} w_{G_z} \sum\limits_{s=1}^{3} \left(\frac{1}{4}(|\sigma_s| + \sigma_s)\cdot\varepsilon_s\right)_{G_xG_yG_z}}{\sum\limits_{G_x=1}^{N_G} w_{G_x} \sum\limits_{G_y=1}^{N_G} w_{G_y} \sum\limits_{G_z=1}^{N_G} w_{G_z}}, \tag{9}$$

$$SED_{\mathrm{C}} = \frac{\sum\limits_{G_x=1}^{N_G} w_{G_x} \sum\limits_{G_y=1}^{N_G} w_{G_y} \sum\limits_{G_z=1}^{N_G} w_{G_z} \sum\limits_{s=1}^{3} \left(\frac{-1}{4}(|\sigma_s| - \sigma_s)\cdot\varepsilon_s\right)_{G_xG_yG_z}}{\sum\limits_{G_x=1}^{N_G} w_{G_x} \sum\limits_{G_y=1}^{N_G} w_{G_y} \sum\limits_{G_z=1}^{N_G} w_{G_z}}, \tag{10}$$

where N_G is the number of one-dimensional Gaussian integral points in the isoparametric element.

The tensile modulus of the rth material should be chosen and evaluated from (9) when $\sigma_1 > \sigma_2 > \sigma_3 \geq 0$. If $0 \geq \sigma_1 > \sigma_2 > \sigma_3$, the compressive modulus should be chosen and evaluated from (10). Under a complex stress state, i.e., $\sigma_1 \cdot \sigma_3 < 0$, the elastic modulus depends on the comparison between the values of the tension SED and compression SED, which considers the influence of the second principal stress.

Equations (9–10) also indicate that modulus selection is independent of the material number of all the m bi-modulus materials. Briefly, either all the tensile moduli or all the compressive moduli are chosen, simultaneously.

3.3.2 Modification of local stiffness

Before modification of the local stiffness of the jth finite element, two types of SED are carried out. One is the "**new**" SED of the element under the complex stress state at the kth iteration of updating of the design variables, i.e.,

$$SED_{j,k} = \frac{\left.\sum_{G_x=1}^{N_G} w_{G_x} \sum_{G_y=1}^{N_G} w_{G_y} \sum_{G_z=1}^{N_G} w_{G_z} \sum_{s=1}^{3} \left(\frac{1}{2}\sigma_s \cdot \varepsilon_s\right)\right|_{G_x G_y G_z}}{\sum_{G_x=1}^{N_G} w_{G_x} \sum_{G_y=1}^{N_G} w_{G_y} \sum_{G_z=1}^{N_G} w_{G_z}}. \tag{11}$$

The other is the "**old**" SED or the effective SED of the element with the original bi-modulus materials under the same stress state, which is defined as

$$SED_{j,k}^{\text{effective}} = \sum_{r=1}^{m} \left\{ \psi_r \cdot \frac{\left.\sum_{G_x=1}^{N_G} w_{G_x} \sum_{G_y=1}^{N_G} w_{G_y} \sum_{G_z=1}^{N_G} w_{G_z} \sum_{s=1}^{3} \left(\frac{1}{2}\text{sign}_r(\sigma_s)\sigma_s \cdot \varepsilon_s\right)\right|_{G_x G_y G_z}}{\sum_{G_x=1}^{N_G} w_{G_x} \sum_{G_y=1}^{N_G} w_{G_y} \sum_{G_z=1}^{N_G} w_{G_z}} \right\}_{j,k} \tag{12}$$

where ψ_r denotes the proportion of the rth material in the element. The value of $\text{sign}_r(\cdot)$ can be calculated using either (13) or (14).

(a) If the element has ***compressive moduli*** at the (k-1)th iteration and ***tensile moduli*** should be used at the current kth iteration, we have

$$\text{sign}_r(\sigma_s) = \begin{cases} 1 & \text{if} \sigma_s \geq 0 \\ R_{\text{TCE}}^{(r)} & \text{if } \sigma_s < 0 \end{cases} \tag{13}$$

where $R_{\text{TCE}}^{(r)}$ is the moduli ratio of the rth bi-modulus material.

(b) If the element has ***tensile moduli*** at the (k-1)th iteration and ***compressive moduli*** should be used at the current kth iteration, we have

$$\text{sign}_r(\sigma_s) = \begin{cases} 1 & \text{if} \sigma_s \leq 0 \\ \left(R_{\text{TCE}}^{(r)}\right)^{-1} & \text{if} \sigma_s > 0 \end{cases} \tag{14}$$

By comparing (11) and (12), we find that the two SEDs are identical when the element is under a pure tension or pure compression state. If the element is under a complex stress state, the two SEDs are usually different. The degree of difference is defined as

$$M_f = \max\left(10^{-6}, \frac{SED_{j,k}^{\text{effective}}}{\max\left(SED_{j,k}, 10^{-10}\right)}\right) \tag{15}$$

for the local effective stiffness of the jth element at the kth iteration.

The stiffness matrix of the jth element with "new" isotropic materials can be given as

$$\boldsymbol{k}_j = \int_{v_j} \boldsymbol{B}_j^T \boldsymbol{D}_j \boldsymbol{B}_j dv \tag{16}$$

where $\boldsymbol{B}_j$ is the strain–displacement operator of the element. $\boldsymbol{D}_j$ is the elasticity matrix of the element with the multiple isotropic materials whose equivalent elastic modulus is given in (7).

The modified stiffness matrix is expressed as:

$$\overline{\boldsymbol{k}}_j = M_f \boldsymbol{k}_j = \int_{v_j} \boldsymbol{B}_j^T \left(M_f \cdot \boldsymbol{D}_j\right) \boldsymbol{B}_j dv. \tag{17}$$

Fig. 3 Initial design domain of a deep cantilever beam with its optimal material layouts in three different cases

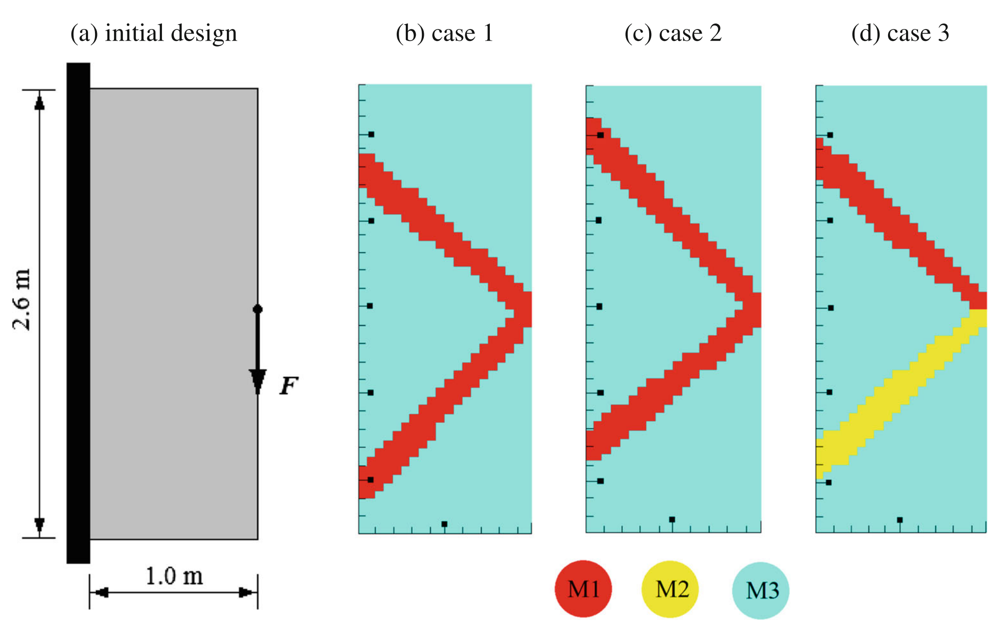

Table 1 Parameters of materials in structure

Material no.		Material 1 (M1)	Material 2 (M2)	Material 3 (M3)
Tensile modulus		200e9 Pa	100e9 Pa	1e–6 Pa
R_{TCE}	Case 1	0.5	1	1 (isotropic)
	Case 2	2	1	1
	Case 3	2	0.5	1
Volume Ratio	Case 1	0.16	**0**	0.84
	Case 2	0.16	**0**	0.84
	Case 3	0.08	0.08	0.84

The modification of the local stiffness can also be understood as a constant that provides secondary adjustment to the design variables in the *j*th element, and is used for calculating the objective function.

In (4), the objective function is modified as

$$\overline{c} = \sum_j \boldsymbol{u}_j^T \left(M_f \boldsymbol{k}_j\right) \boldsymbol{u}_j = \sum_j M_f \cdot \boldsymbol{u}_j^T \boldsymbol{k}_j \boldsymbol{u}_j. \tag{18}$$

3.4 Sensitivity analysis

The gradient-based method is used to solve the optimization problem defined in (4). For simplicity, the sensitivity analysis of the model is carried out with the three-phase bi-modulus materials only.

For m=3 (two solids and a void are also possible), the stiffness matrix of the *j*th finite element is

$$\boldsymbol{k}_j = \left[\rho_{2,j}^p\left(\rho_{1,j}^p E_{1,j} + \left(1-\rho_{1,j}^p\right)E_{2,j}\right) + \left(1-\rho_{2,j}^p\right)E_{3,j}\right]\boldsymbol{k}_0 = A_0\boldsymbol{k}_0. \tag{19}$$

where $\boldsymbol{k}_0$ is the stiffness matrix of the *j*th finite element with the identity modulus of isotropic material.

Hence, the first order sensitivity of the stiffness matrix of the *j*th element can be expressed as

$$\frac{\partial \boldsymbol{k}_j}{\partial \rho_{1,j}} = \left(p\rho_{1,j}^{p-1}\cdot\rho_{2,j}^p\cdot E_{1,j} - p\rho_{1,j}^{p-1}\cdot\rho_{2,j}^p\cdot E_{2,j}\right)\boldsymbol{k}_0 = A_1\boldsymbol{k}_0 = \frac{A_1}{A_0}\boldsymbol{k}_j \tag{20}$$

$$\frac{\partial \boldsymbol{k}_j}{\partial \rho_2} = \left\{p\rho_{2,j}^{p-1}\left[\rho_{1,j}^p E_{1,j} + \left(1-\rho_{1,j}^p\right)E_{2,j}\right] + \left(-p\rho_{2,j}^{p-1}\right)E_{3,j}\right\}\boldsymbol{k}_0 = \frac{A_2}{A_0}\boldsymbol{k}_j. \tag{21}$$

Thus, we can obtain the equation

$$\begin{pmatrix} \frac{\partial \overline{c}}{\partial \rho_1} & \frac{\partial \overline{c}}{\partial \rho_2} \end{pmatrix}_j = \left(\begin{pmatrix} \frac{\partial M_f}{\partial \rho_1} & \frac{\partial M_f}{\partial \rho_2} \end{pmatrix} - M_f\begin{pmatrix} \frac{A_1}{A_0} & \frac{A_2}{A_0} \end{pmatrix}\right)_j \cdot \boldsymbol{u}_j^T \boldsymbol{k}_j \boldsymbol{u}_j. \tag{22}$$

It is noted that M_f in (15) indicates the core of the material replacement. Hence, we set $\frac{\partial M_f}{\partial \rho_1} = \frac{\partial M_f}{\partial \rho_2} = 0$ in the present study.

The volume constraint functions can also be defined as

$$\begin{cases} V_1(\rho_1,\ \rho_2) = \sum_{j=1}^n \rho_{1,j}\cdot\rho_{2,j}\cdot v_j - \overline{V}_1, \\ V_2(\ \rho_2) \ = \sum_{j=1}^n \rho_{2,j}\cdot v_j - \left(\overline{V}_1 + \overline{V}_2\right) \end{cases} \tag{23}$$

and the sensitivities of the volume constraints are

$$\begin{pmatrix} \frac{\partial V_1}{\partial \rho_1} & \frac{\partial V_1}{\partial \rho_2} \\ \frac{\partial V_2}{\partial \rho_1} & \frac{\partial V_2}{\partial \rho_2} \end{pmatrix}_j = \begin{pmatrix} \rho_2 v_j & \rho_1 v_j \\ 0 & v_j \end{pmatrix} \tag{24}$$

3.5 Optimization procedure

In the present study, the method of moving asymptotes (MMA) (Svanberg 1987) is adopted to update the design variables. The partial differential equations (PDEs) are solved by the finite element method (FEM). The initial equivalent elastic moduli of elements are the same as the tensile modulus of the first phase material (M1). All the initial values of $\rho_{1,j}$ are set to be the same to $\overline{V}_i/V_\Omega$. V_Ω is the volume of design domain. The optimization processes are as follows:

1) Build finite element model for structural optimization;
2) Initialize the design domain and parameters, let k=1;
3) Calculate the deformation of structure with N_G=2;
4) Calculate the SED and local effective SED ((12)), to obtain M_f according to (15);
5) Calculate the values of the objective ((18)) and constraint functions ((23)) and their sensitivities ((22) and (24));

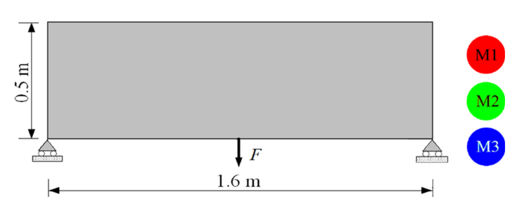

Fig. 4 Initial design domain of a simply supported beam with three different materials, M1, M2, and M3 (void)

Table 2 Parameters of materials in the structure

Material No.	Material 1		Material 2		Material 3 (void)	
Volume Ratio	0.16		0.16		0.68	
Moduli	E_T/GPa	E_C/GPa	E_T/GPa	E_C/GPa	E_T/GPa	E_C/GPa
Case 1	100	100	50	50	1e–15	1e–15
Case 2	100	50	50	100	1e–15	1e–15
Case 3	50	100	100	50	1e–15	1e–15
Case 4	100	200	50	25	1e–15	1e–15

6) Update the design variables and the elastic moduli of the materials in each element;
7) Check the convergence: if the convergence criterion (25) is not satisfied or if k is not higher than the maximum iteration, let $k=k+1$, return to 3), else go to 8);
8) Save and stop.

The convergence criterion is defined according to the change of objective function

$$\left|\frac{\overline{c}_t}{\overline{c}_k}-1\right|\leq\eta,\quad t=k-1,k-2,\quad \ldots,\quad k-n. \tag{25}$$

The tolerance η is 0.01, n is 5, and the maximum number of iterations is 100 in the present study.

4 Numerical examples and discussion

The code for optimization analysis of the present method is compiled using MATLAB and ANSYS(2013). Only the stiffness design with volume constraints on multiple bi-modulus materials is considered. The Poisson's ratio is 0.2 in all cases.

4.1 Example 1— validation test

Figure 3a shows the initial design of a deep cantilever beam structure with thickness of 0.1 m. The design domain is meshed with 20×52 plane stress elements. The left side of the structure is fixed. A concentrated force, $F=1.0$ kN, is applied at the center of the right side. The volume constraint of the solid phase is 16 %. There are two solids and a void phase (material 3) in the structure. Three cases are considered. In cases 1 and 2, the volume ratio of material 2 is zero, which means that single phase layout optimization is considered with different values of R_{TCE} of material 1. In case 3, two solids are used in the structure. The detailed parameters are listed in Table 1.

From Table 1, we know that there is only one bi-modulus material and void phase in the structure for the first and the second cases. For case 1, the value of R_{TCE} is 0.5, which means that the material tensile modulus is half of the compressive modulus. Hence, the amount of material under compression should be higher than that under tension. Figure 3b gives the final bi-modulus material layout, which has been verified in our previous work (Cai et al. 2014c). For the second case, the optimal material layout is shown in Fig. 3c, which is symmetric with that in Fig. 3b due to the value of R_{TCE} being 2.0.

For the third case, there are two solids with the same volume ratio in the final structure. In this case, the moduli of M1 are 200 and 100 GPa for E_{C} and E_{T}, respectively, and the moduli of M2 are 100 and 200 GPa, respectively. Therefore, the optimal material layout in Fig. 3d is symmetric because the moduli of the two materials are the same.

4.2 Example 2— sensitivity of material distribution to R_{TCE}

The structure shown in Fig. 4 is a simply supported rectangular beam with length of 1.6 m, height of 0.5 m, and thickness of 0.01 m. A concentrated force, $F=4$ kN, is applied vertically at the center of the lower side.

In the present example, three materials are used in the structure. Four cases of bi-modulus material layout schemes are considered. The relevant parameters are listed in Table 2.

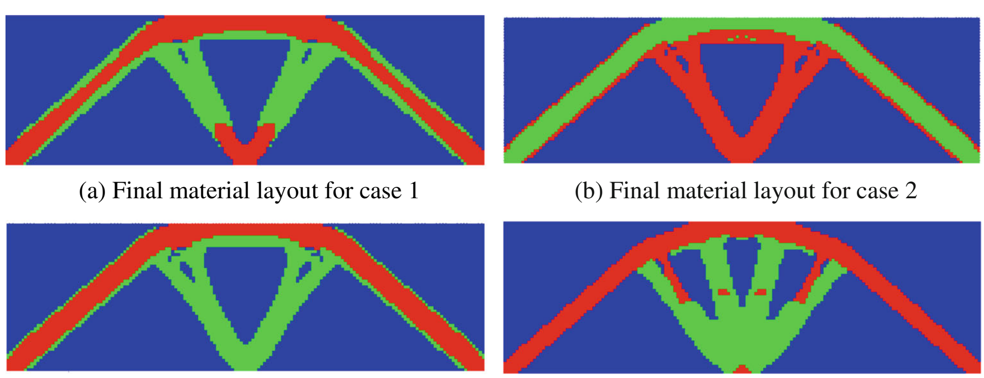

(a) Final material layout for case 1 (b) Final material layout for case 2 (c) Final material layout for case 3 (d) Final material layout for case 4

Fig. 5 Optimal material layouts in structure for different schemes (M1 in *red*, M2 in *green* and M3 in *blue*)

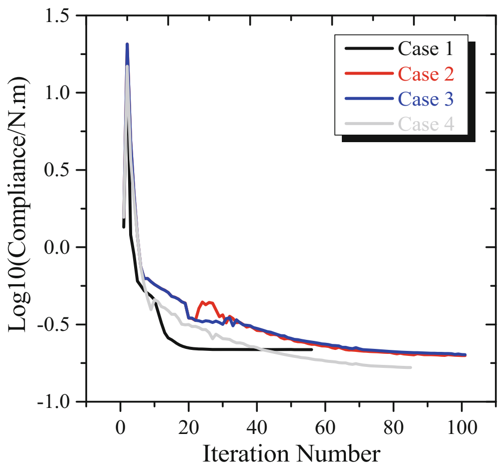

Fig. 6 Iteration histories of structural compliance (logarithm) for the four cases

The optimal multiple-material layout results are shown in Fig. 5. For the first case, M1 and M2 are isotropic materials and the third is void; Fig. 5a shows their final layout in the design domain. Two legs supporting a triangle component are under compression. Besides the two legs, the top side of the triangle is also made of M1. M2 is mainly under tension in the structure. Due to higher volume ratio of M2, a part of M2 is coated on the two red legs to improve the stiffness of structure. When the volume ratio of M1 is higher or the volume ratio of M2 becomes lower, the interface between M1 and M2 will become simple.

Figure 5b gives the final layout of two bi-modulus materials in case 2. As the tensile modulus of M1 is equal to the compressive modulus of M2, i.e., 100 Gpa, and the compressive modulus of M1 is identical to the tensile modulus of M2, i.e., 50 GPa, the M2 is almost entirely laid out in the compression zone in the structure. Also, M1 is under tension, which is used to support the concentrated load.

In case 3, the two materials, M1 and M2, are the same as M2 and M1 in case 1, respectively. Therefore, we find that Fig. 5c gives the same topology but a different material layout scheme compared to that in Fig. 5b.

In case 4, both moduli of M1 are much higher than the moduli of M2. Hence, M1 is mainly under compression and M2 is under tension due to their same volume ratio but different span of material distribution in structure.

It is concluded that the final topology of a structure with many bi-modulus materials is determined not only by the values of R_{TCE} but also by the moduli differences among materials. In particular, at a location with a concentrated load, the material with higher modulus will easily be used when the local deformation is complex. Therefore, in Fig. 5a and d we find isolated M1 (with higher modulus) coated with M2.

As mentioned in Section 3.5, there is only the first phase material (M1) in the elements in design domain, the initial structural compliance is so high obviously. In optimization, there are 54 updates for design domains and the final structural compliance reaches 0.2173 N.m for the first case (Fig. 6) by SIMP method. For case 2 and case 3, the values of structural compliance approach 0.1989 and 0.2018 N.m, respectively. The compliance difference between the two cases is mainly due to reaching the maximum iteration, 100 in this study. From Fig. 6, we find that the objectives are very close to each other for the two cases when the number of iterations exceeds 40. In case 4, 84 iterations are required before the structural compliance converges to 0.1665 N.m. The lower number of iterations demonstrates that the efficiency of the present method is high.

4.3 Example 3—a mid-supported bridge

The initial design of a mid-supported bridge is a rectangle zone (Fig. 7) with the span of 19.2 m and height of 4.8 m. A uniform pressure of P=20 kN/m is applied vertically on the bridge floor with thickness of 0.1 m. The floor is a non-design domain which is located 1.6 m above the bottom of bridge (see Fig. 7). The two sides of each bottom corner are fixed with length 1.2 m. The structure is discretized using 192×48 plane stress elements. The material in the bridge floor is labeled M4 with modulus of 40 GPa (of a type of concrete). Volume constraint is imposed in this example. Stiffness design with volume constraints is considered and the related parameters are listed in Table 3.

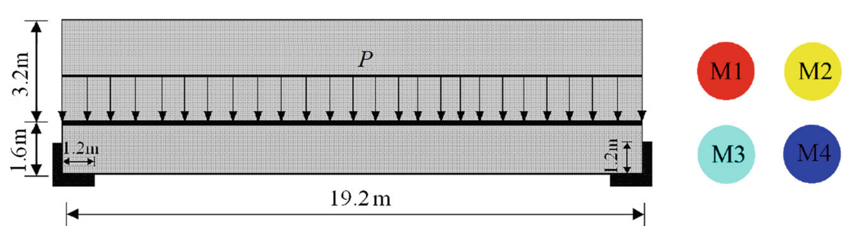

Fig. 7 Design domain of a bridge with four materials, M1, M2 and M3 are in the design domain, M4 is the bridge floor, which is the non-design domain during optimization

Table 3 Parameters of materials in structure

Material No.	Material 1		Material 2		Material 3 (void)	
Volume ratio	0.1		0.2		0.7	
Moduli of	E_T/GPa	E_C/GPa	E_T/GPa	E_C/GPa	E_T/GPa	E_C/GPa
Case 1	200	200	80	80	1e–15	1e–15
Case 2	200	200	40	80	1e–15	1e–15
Case 3	200	200	4	80	1e–15	1e–15
Case 4	200	10	40	80	1e–15	1e–15

Figure 8 presents four designs of a mid-supported bridge with different materials. In Fig. 8a, the two solids (M1 in red and M2 in green) are isotropic materials. Because of the higher modulus value, M1 is used in the higher stress zone. The greatest amount of M2 is in the zone over the floor. Due to excellent tensile property of M2, the mid-section of the floor is connected with M2, which is under tension state.

In Fig. 8b (corresponding to case 2), M1 is still an isotropic material, but M2 is a bi-modulus material with lower tensile modulus. Therefore, a small amount of M2 is under the floor to provide effective support. Meanwhile, the amount of M1 above the floor is greater than that in Fig. 8a. The shape of M2 above the floor is also slightly different from that in Fig. 8a.

In case 3, M2 is a bi-modulus material in which the tensile modulus is far less than the compressive modulus, and can be considered approximately as a compression-only material (Cai 2011). Thus we find in Fig. 8c that the mid-section of the floor is supported by M1, which resembles links connecting the floor and the major arch of M2.

In case 4, M1 and M2 are bi-modulus materials. The compressive modulus (10 GPa) of M1is far less than its tensile modulus (200 GPa). It is reasonable, therefore, to consider M1 as a tension-only material. In Fig. 8d we find that M1 plays the major role in stretching across most of the bridge floor. Simultaneously, the whole of M2 is under compression due to its weaker tensile modulus.

In the above four results, only stiffness design is considered and the strength difference of M2 (concrete) is not considered. Thus, the designs in Fig. 8a and b are not rational when M2 is a real concrete in practical engineering. However, the designs in Fig. 8c and d are acceptable before the sizing or shape design of the bridge. We conclude that bi-modulus behavior has a vital influence on the final material layout in structures with many solids.

5 Conclusions

In consideration of the wide application of bi-modulus materials in practical engineering, we have presented here a modified SIMP method for deriving the optimal stiffness design of a structure with multiple bi-modulus materials. Three typical numerical examples were considered to assess the applicability and efficiency of the present algorithm. Based on the numerical results obtained, some conclusions are drawn:

(1) The algorithm is available for achieving single bi-modulus material topology optimization in a structure from the first draft, and the final structure may be symmetric when two bi-modulus materials are used in the structure;
(2) The final topology of a structure with many bi-modulus materials depends on the values of R_{TCE}, the amount of materials and the moduli differences among materials. At locations with highly complex stress states, the material with higher modulus will be readily used;
(3) If the moduli of a bi-modulus material are significantly different, that material will be laid out under either almost pure tension or almost pure compression in the final structure.

Fig. 8 Optimal material layouts in the bridge with different bi-modulus materials

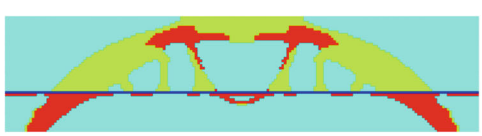

(a) Final material layout for case 1

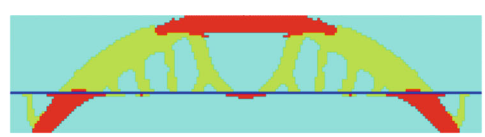

(b) Final material layout for case 2

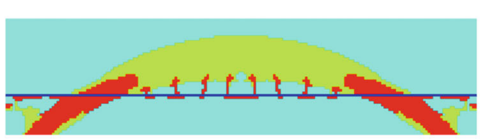

(c) Final material layout for case 3

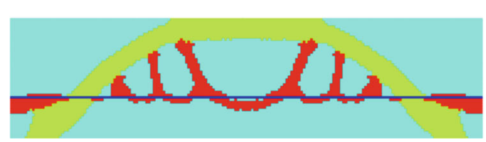

(d) Final material layout for case 4

Acknowledgments Financial support from the National Natural-Science-Foundation of China (Nos. 51279171 and 11372100) and Australian Research Council (No. DP140103137) is gratefully acknowledged.

References

Achtziger W (1996) Truss topology optimization including bar properties different for tension and compression. Struct Optim 12(1):63–74

Alfieri L, Bassi D, Biondini F, Malerba PG (2007) Morphologic evolutionary structural optimization. 7th world congress on structural and multidisciplinary optimization Seoul, Korea, paper A

Allaire G, Jouve F, Toader A-M (2004) Structural optimization using sensitivity analysis and a level-set method. J Comput Phys 194(1): 363–393

Allaire G, Dapogny C, Delgado G, Michailidis G (2014) Multi-phase structural optimization via a level set method. Esaim Control Optim Calculus Var 20(2):576–611

Ambartsumyan S (1965) The axisymmetric problem of circular cylindrical shell made of materials with different stiffness in tension and compression. Izvestiya Akademiya Nauk SSSR. Mekhanika 4: 77-85

Andreasen CS, Gersborg AR, Sigmund O (2009) Topology optimization of microfluidic mixers. Int J Numer Methods Fluids 61(5):498–513

Ansys (2013) Ansys. Ansys. http://www.ansyscom, 2013. Assessed April 2015

Baratta A, Corbi I, Corbi O (2015) Analytical formulation of generalized incremental theorems for 2D no-tension solids. Acta Mech. doi:10.1007/s00707-015-1350-2

Bathe K-J (2006) Finite element procedures. Klaus-Jurgen Bathe, United States of America

Bendsoe MP, Sigmund O (2003) Topology optimization: theory, methods and applications. Springer Science & Business Media

Blasques JP, Stolpe M (2012) Multi-material topology optimization of laminated composite beam cross sections. Compos Struct 94(11): 3278–3289

Bruggi M (2014) Finite element analysis of no-tension structures as a topology optimization problem. Struct Multidiscip Optim 50(6): 957–973

Bruggi M, Duysinx P (2013) A stress-based approach to the optimal design of structures with unilateral behavior of material or supports. Struct Multidiscip Optim 48(2):311–326

Cai K (2011) A simple approach to find optimal topology of a continuum with tension-only or compression-only material. Struct Multidiscip Optim 43(6):827–835

Cai K, Qin QH (2012) A new construction method for a lightweight submerged radial gate. Front Eng Mech Res 1(1):1–7

Cai K, Qin QH, Luo Z, Zhang A (2013) Robust topology optimisation of bi-modulus structures. Comput Aided Des 45(10):1159–1169

Cai K, Gao DY, Qin QH (2014a) Postbuckling analysis of a nonlinear beam with axial functionally graded material. J Eng Math 88:121–136

Cai K, Gao DY, Qin QH (2014b) Postbuckling solutions of hyper-elastic beam by canonical dual finite element method. Math Mech Solids 19(6):659–671

Cai K, Gao Z, Shi J (2014c) Topology optimization of continuum structures with bi-modulus materials. Eng Optim 46(2):244–260

Cai K, Luo ZJ, Qin QH (2014d) Topology optimization of bi-modulus structures using the concept of bone remodeling. Eng Comput 31(7): 1361–1378

Chang C, Zheng B, Gea H (2007) Topology optimization for tension/compression only design. Proceedings of the 7th world congress on structural and multidisciplinary optimization. pp 2488–2495

Diaz AR, Sigmund O (2010) A topology optimization method for design of negative permeability metamaterials. Struct Multidiscip Optim 41(2):163–177

Dorn WS (1964) Automatic design of optimal structures. J Mecanique 3: 25–52

Du Z, Guo X (2014) Variational principles and the related bounding theorems for bi-modulus materials. J Mech Phys Solids 73:183–211

Dühring MB, Jensen JS, Sigmund O (2008) Acoustic design by topology optimization. J Sound Vib 317(3):557–575

Eschenauer HA, Olhoff N (2001) Topology optimization of continuum structures: a review*. Appl Mech Rev 54(4): 331–390

Gibiansky LV, Sigmund O (2000) Multiphase composites with extremal bulk modulus. J Mech Phys Solids 48(3):461–498

Guan H, Steven G, Xie M (1999) Evolutionary structural optimisation incorporating tension and compression materials. Adv Struct Eng 2: 273–288

Guo X, Zhang W, Zhong W (2014a) Stress-related topology optimization of continuum structures involving multi-phase materials. Comput Methods Appl Mech Eng 268:632–655

Guo X, Zhang W, Zhong W (2014b) Doing topology optimization explicitly and geometrically—a new moving morphable components based framework. J Appl Mech 81(8):081009

Han S-Y, Lee S-K (2005) Development of a material mixing method based on evolutionary structural optimization. JSME Int J Ser A 48(3):132–135

Huang X, Xie M (2010) Evolutionary topology optimization of continuum structures: methods and applications. Wiley

Hvejsel CF, Lund E (2011) Material interpolation schemes for unified topology and multi-material optimization. Struct Multidiscip Optim 43(6):811–825

Jones RM (1977) Stress-strain relations for materials with different moduli in tension and compression. AIAA J 15(1):16–23

Kanno Y (2011) Nonsmooth mechanics and convex optimization. CRC Press

Liu S, Qiao H (2011) Topology optimization of continuum structures with different tensile and compressive properties in bridge layout design. Struct Multidiscip Optim 43(3):369–380

Liu Y, Xie Z, Van Humbeeck J, Delaey L (1998) Asymmetry of stress–strain curves under tension and compression for NiTi shape memory alloys. Acta Mater 46(12):4325–4338

Luo Z, Tong L, Ma H (2009) Shape and topology optimization for electrothermomechanical microactuators using level set methods. J Comput Phys 228(9):3173–3181

Maute K, Frangopol DM (2003) Reliability-based design of MEMS mechanisms by topology optimization. Comput Struct 81(8):813–824

Mei Y, Wang X (2004) A level set method for structural topology optimization with multi-constraints and multi-materials. Acta Mech Sinica 20(5):507–518

Mosler J, Cirak F (2009) A variational formulation for finite deformation wrinkling analysis of inelastic membranes. Comput Methods Appl Mech Eng 198(27):2087–2098

Norato JA, Bell BK, Tortorelli DA (2015) A geometry projection method for continuum-based topology optimization with discrete elements. Comput Methods Appl Mech Eng 293:306–327

Osher SJ, Santosa F (2001) Level set methods for optimization problems involving geometry and constraints: I. frequencies of a two-density inhomogeneous drum. J Comput Phys 171(1):272–288

Qin QH (2000) The Trefftz finite and boundary element method. WIT PRESS, Southampton

Qin QH (2005) Trefftz finite element method and its applications. Appl Mech Rev 58(5):316–337

Qin QH, Ye JQ (2004) Thermoelectroelastic solutions for internal bone remodeling under axial and transverse loads. Int J Solids Struct 41(9):2447–2460

Qin QH, Qu C, Ye JQ (2005) Thermoelectroelastic solutions for surface bone remodeling under axial and transverse loads. Biomaterials 26 (33): 6798–6810

Querin OM, Victoria M, Martí P (2010) Topology optimization of truss-like continua with different material properties in tension and compression. Struct Multidiscip Optim 42(1):25–32

Ramani A (2010) A pseudo-sensitivity based discrete-variable approach to structural topology optimization with multiple materials. Struct Multidiscip Optim 41(6):913–934

Roddeman D, Drukker J, Oomens C, Janssen J (1987) The wrinkling of thin membranes: part I—theory. J Appl Mech 54(4):884–887

Rodriguez-Velazquez J, Seireg A (1985) Optimizing the shapes of structures via a rule-based computer program. Comput Mech Eng 4(1):20–28

Rozvany G, Bendsoe M, Kirsch U (1995) Layout optimization of structures. Appl Mech Rev 48(2):41–119

Seldin EJ (1966) Stress-strain properties of polycrystalline graphites in tension and compression at room temperature. Carbon 4(2):177–191

Shi J, Cai K, Qin QH (2014) Optimal mass distribution prediction for human proximal femur with bi-modulus property. Mol Cell Biomech 11(4):235–248

Sigmund O (1994) Materials with prescribed constitutive parameters: an inverse homogenization problem. Int J Solids Struct 31(17):2313–2329

Sigmund O, Torquato S (1999) Design of smart composite materials using topology optimization. Smart Mater Struct 8(3):365

Stegmann J, Lund E (2005) Discrete material optimization of general composite shell structures. Int J Numer Methods Eng 62(14): 2009–2027

Stimpson B, Chen R (1993) Measurement of rock elastic moduli in tension and in compression and its practical significance. Can Geotech J 30(2):338–347

Svanberg K (1987) The method of moving asymptotes—a new method for structural optimization. Int J Numer Methods Eng 24(2):359–373

Wang MY, Wang X (2004) "Color" level sets: a multi-phase method for structural topology optimization with multiple materials. Comput Methods Appl Mech Eng 193(6):469–496

Wang MY, Zhou S (2004) Synthesis of shape and topology of multi-material structures with a phase-field method. J Computer-Aided Mater Des 11(2–3):117–138

Wang MY, Wang X, Guo D (2003) A level set method for structural topology optimization. Comput Methods Appl Mech Eng 192(1): 227–246

Wang Y, Luo Z, Kang Z, Zhang N (2015) A multi-material level set-based topology and shape optimization method. Comput Methods Appl Mech Eng 283:1570–1586

Xiao Y, Qin QH (2013) Cell based full field displacement calculation for foam material. Proc SIF 2013

Xie YM, Steven GP (1993) A simple evolutionary procedure for structural optimization. Comput Struct 49(5):885–896

Xie YM, Steven GP (1997) Basic evolutionary structural optimization. Springer

Yang Y, Moen CD, Guest JK (2015) Three-dimensional force flow paths and reinforcement design in concrete via stress-dependent truss-continuum topology optimization. J Eng Mech 141(1):04014106

Zenkert D, Burman M (2009) Tension, compression and shear fatigue of a closed cell polymer foam. Compos Sci Technol 69(6):785–792

Zhou M, Rozvany G (1991) The COC algorithm, part II: topological, geometrical and generalized shape optimization. Comput Methods Appl Mech Eng 89(1):309–336

Zhou S, Wang MY (2007) Multimaterial structural topology optimization with a generalized Cahn–Hilliard model of multiphase transition. Struct Multidiscip Optim 33(2):89–111

Zhu L, Zhao H, Song Y (2006) Experimental investigation of the mechanical properties of Takin femoral cortical bone. J Tsinghua Univ 46(2):301

Zhuang C, Xiong Z, Ding H (2007) A level set method for topology optimization of heat conduction problem under multiple load cases. Comput Methods Appl Mech Eng 196(4):1074–1084

Zhuang C, Xiong Z, Ding H (2010) Topology optimization of multi-material for the heat conduction problem based on the level set method. Eng Optim 42(9):811–831